J Mol Model (2013) 19:1527–1536
DOI 10.1007/s00894-012-1714-7

ORIGINAL PAPER

# Probing the structural, electronic and magnetic properties of multicenter $Fe_2S_2^{0/-}$, $Fe_3S_4^{0/-}$ and $Fe_4S_4^{0/-}$ clusters

**Li-Ping Ding · Xiao-Yu Kuang · Peng Shao · Ming-Min Zhong**

Received: 17 August 2012 / Accepted: 27 November 2012 / Published online: 21 December 2012


**Abstract** The structural, electronic and magnetic properties of neutral and anion $Fe_2S_2$, $Fe_3S_4$ and $Fe_4S_4$ have been investigated with the aid of previous photoelectron spectroscopy and density functional theory calculations. Theoretical electron detachment energies (both vertical and adiabatic) of anion clusters for the lowest energy structure were computed and compared with the experimental results to verify the ground states. The optimized structures show that the ground state structures of $Fe_2S_2^{0/-}$, $Fe_3S_4^{0/-}$ and $Fe_4S_4^{0/-}$ favor high spin state and are similar to their structures in proteins. The electron delocalization pattern for all the clusters and the nature of bonding between Fe and S atoms were studied by analyzing molecular orbitals. Natural population analysis demonstrates that Fe atoms act as an electron donor in all clusters, and the electron density difference map clearly shows the direction of the electron flow over the whole complex. Furthermore, the investigated magnetism shows that the Fe atoms carried most of the magnetic moments, which is due mainly to the 3d state, while only very small magnetic moments are found on S atoms.

**Keywords** Fe-S cluster · Photoelectron spectroscopy · Density functional theory · Magnetic properties

## Introduction

Iron–sulfur (Fe-S) clusters can be considered an interface between the biological and inorganic worlds [1]. Biological Fe-S clusters are among the most ancient, ubiquitous and functionally diverse prosthetic group in all of biology [2–6]. Fe-S-cluster-containing proteins are especially widely distributed in nonphotosynthetic, aerobic bacteria, higher plants and animals [7]. Meanwhile, complex Fe-S-cluster-containing enzymes, a common feature of which is that their catalytically active center is comprised not of a single iron atom but of several Fe atoms bound to sulfur [8–11], are involved in a number of fundamental processes required for life, such as carbon monoxide oxidation, carbon dioxide fixation, nitrogen fixation and hydrogen metabolism [12]. To date, in excess of 120 distinct types of enzymes and proteins are known with $Fe_2S_2$, cubane-type $Fe_3S_4$ and $Fe_4S_4$ units that act as active centers in various proteins. The $Fe_2S_2$, $Fe_3S_4$ and $Fe_4S_4$ clusters are multicenter clusters and are also found in ferredoxins [11]. These three clusters are connected to the protein backbone by cysteine ligands (Cys). And they undergo some oxidation–reduction reactions that can influence protein structure by preferential side chain ligation. In addition to their electron transfer function, Fe-S clusters act as catalytic centers and sensors of iron and oxygen, as described previously [3].

As a first step towards understanding the intrinsic electronic properties of Fe-S active centers, naked iron sulfur ($Fe_2S_2$, $Fe_3S_4$ and $Fe_4S_4$) clusters have been studied in some experimental works. Nakajimas's study [13] on Fe-S in the gas phase depicted the electronic and geometric properties of Fe-S clusters ($Fe_nS_m$, $n$=1-8, $m$=2–6) using photoelectron spectroscopy (PES); their results also show that $Fe_nS_m$ clusters seemingly adopt a structure having alternate bonds between Fe and S atoms, which will be again confirmed by our work. PES studies on anionic Fe-S clusters were performed by Zhang's group [14] and the results showed that stable $Fe_nS_m^-$ clusters are those with the composition $n=m$ and $n=m\pm1$, indicating that $Fe_nS_m^+$ clusters with $n$=2, 3, 4 and 6 are the stable species in the gas phase. Furthermore, their corresponding electron affinities (EA) and vertical detachment energies (VDE) have been obtained from

L.-P. Ding · X.-Y. Kuang · P. Shao · M.-M. Zhong
Institute of Atomic and Molecular Physics, Sichuan University, Chengdu 610065, China

X.-Y. Kuang (✉)
International Centre for Materials Physics, Academia Sinica, Shenyang 110016, China
e-mail: scu_kuang@163.com

photoelectron spectra of isolated larger anionic clusters [14]. It is worth pointing out that cationic $Fe_nS_m^+$ clusters have been generated by reaction of $Fe_n^+$ with $CS_2^-$ [15]. Similarly, neutral $Fe_nS_m$ clusters are observed as a reaction product of $Fe_n$ and $H_2S$ ($Fe_n$+ $H_2S \rightarrow Fe_nS$) [16]. Indeed, these detailed experiments of the Fe-S complexes are useful for calibrating computational investigations.

To our knowledge, most theoretical calculations to date have been devoted to Fe-S clusters in protein environments [17–22] and in a wide range of metal cubanes (e.g., $[(C_5H_5)_4Fe_4S_4]^{2+}$) [23]. Some quantum chemical calculations reported a model of clusters that contain additional ligands surrounding $Fe_2S_2$ and $Fe_4S_4$. However, there have been relatively few detailed studies of the electronic and geometric structures of neutral or charged $Fe_2S_2$, $Fe_3S_4$ and $Fe_4S_4$ isolated species. The chemical bonding of the latter is still not well understood because the electrons of the iron atoms in multicenter clusters exhibit a weak magnetic coupling and manifold nearly degenerate states. The iron d–d interaction is quite weak, and the closed-shell solution is unstable to perturbation that allows electron spins to localize at the iron centers. Moreover, one of the difficulties associated with transition metal elements is their open d shell structure. The d electrons are quasi-localized and a cluster containing transition metal atoms has many spin-multiplet structures within a narrow energy range. Thus obtaining the spin multiplicity of the ground state is a nontrivial problem, and it has remained ambiguous so far. Due to the lack of theoretical calculations, the understanding of iron-sulfur clusters in Fe-S protein active sites, and the problem of the spin multiplicity for binary clusters containing a magnetic element, we report here a more extensive and systematical density functional theory (DFT) investigation on neutral and anionic $Fe_2S_2$, $Fe_3S_4$ and $Fe_4S_4$ clusters, but free of any ligands.

The main objectives of this research were: (1) to investigate the true various ground state structures and electronic properties of the bare neutral and anionic $Fe_2S_2$, $Fe_3S_4$ and $Fe_4S_4$ clusters; (2) to compare our extensive computational results with previously experimental and theoretical findings [13, 24–26]; and (3) to determine spin multiplicity of the ground state and increase more databases for experimental and theoretical investigation in the future. Moreover, because hybridization of Fe with the metalloid S atom will modify the magnetic moment on the Fe atom as well as the coupling with the other Fe atom, we are also interested in the magnetic properties of these systems.

This paper is organized as follows: the following section presents a brief description of the Computational details. The calculated properties as well as experimental and theoretical results for the $Fe_2S_2^{0/-}$, $Fe_3S_4^{0/-}$ and $Fe_4S_4^{0/-}$ clusters are discussed in the Results and discussion, followed by Conclusions.

## Computational details

All the clusters were studied using the Gaussian03 program package [27] at the DFT level of theory. As a check, two-atom clusters ($S_2$, $S_2^-$, $Fe_2$, FeS and $FeS^-$) were tested with several exchange-correlation functionals and the same 6-311+G* basis set for accuracy and consistency. The inclusion of polarization and diffuse functions in the 6-311+G* basis set has been shown to be important [28] in calculations involving transition metals at correlated levels, and this basis set has been applied successfully to calculate the structural dichotomy of cationic, anionic, and neutral $FeS_2$ [29]. The results of the tested calculations using the PW91 [30, 31], B3LYP [30, 32], TPSS [33] and PBE [33], and BP86 [32, 34] functionals, which compared with the experimental results [14, 35–44], are summarized in Table 1. In a series of trials, it can be noted that the results for bond lengths ($r$), vibration frequencies ($\omega$), and dissociation energies ($D$) are quite sensitive to the choices of B3PW91 functional that includes the Becke-Perdew-Wang exchange-correlation potential. Here, we consider the FeS and $FeS^-$ molecules as a test case for a theoretical description,

**Table 1** Calculated values of bond length $r$ (Å), frequency $\omega$ ($cm^{-1}$), dissociation energy $D$ (eV) for the $S_2$, $S_2^-$, $Fe_2$, FeS and $FeS^-$ molecules at different level

| Method | Para | Clusters | | | | |
|---|---|---|---|---|---|---|
| | | $S_2$ Multi | $S_2^-$ | $Fe_2$ | FeS | $FeS^-$ |
| | | 3 | 2 | 7 | 5 | 4 |
| PW91 | $r$ | 2.08 | 2.06 | 2.01 | 2.02 | 2.05 |
| | ω | 583 | 526 | 399 | 516 | 470 |
| | $D$ | 4.61 | 1.94 | 2.48 | 4.22 | 3.61 |
| B3LYP | $r$ | 1.93 | 2.05 | 1.98 | 2.01 | 2.09 |
| | ω | 428 | 536 | 428 | 528 | 449 |
| | $D$ | 4.08 | 1.48 | 0.31 | 3.16 | 2.90 |
| TPSS | $r$ | 1.93 | 2.06 | 2.00 | 2.02 | 2.06 |
| | ω | 671 | 528 | 406 | 518 | 469 |
| | $D$ | 4.36 | 1.85 | 1.93 | 4.03 | 3.40 |
| BP86 | $r$ | 1.94 | 2.06 | 2.01 | 2.02 | 2.05 |
| | ω | 660 | 519 | 402 | 515 | 468 |
| | $D$ | 4.57 | 1.75 | 2.39 | 4.15 | 3.52 |
| PBE | $r$ | 1.94 | 2.06 | 2.01 | 2.02 | 2.06 |
| | ω | 667 | 528 | 396 | 515 | 468 |
| | $D$ | 4.61 | 1.96 | 2.47 | 4.20 | 3.60 |
| B3PW91 | $r$ | 1.91 | 2.04 | 1.98 | 2.02 | 2.09 |
| | ω | 706 | 561 | 432 | 525 | 461 |
| | $D$ | 4.19 | 1.68 | 0.80 | 3.69 | 3.18 |
| Experiment | $r$ | 1.89 [36] | | 2.02 [41] | 2.04 [43] | 2.18 [35] |
| | ω | 726 [36] | 589 [38] | 300 [40] | 540 [44] | 450 [35] |
| | $D$ | 4.37 [39] | | 1.14 [42] | 3.31 [37] | 2.99 [14] |

since they are the smallest molecules with an iron–sulfur bond.

To search for low-lying structures of $Fe_2S_2$, $Fe_3S_4$ and $Fe_4S_4$ clusters, the equilibrium geometries of bare $S_4$, $S_7$ and $S_8$ clusters were first optimized based on previous calculated results [45–48]. The isomers of $Fe_2S_2$, $Fe_3S_4$ and $Fe_4S_4$ were searched extensively in two ways: (1) by considering the possible structures reported in previous papers, and (2) by placing some Fe atoms at various substitutional sites on the basis of optimized bare $S_4$, $S_7$ and $S_8$ geometries. For low-lying isomers of anionic species, we also searched extensively using the same method employed for neutral clusters. Additionally, because of the spin polarization, every initial structure was optimized at various possible spin multiplicities, i.e., in our paper, the neutral species $Fe_2S_2$, $Fe_3S_4$ and $Fe_4S_4$ were repeatedly optimized using different spin multiplicities of 1, 3, 5, 7, 9, …, and for the anion cluster using 2, 4, 6, 8, 10, …, until the lowest energy structure was found. Moreover, in order to confirm that the optimized geometry corresponds to a local minimum in potential energy, each was followed by an analysis of harmonic vibration frequencies. In the case of an imaginary frequency, relaxation along the corresponding unstable normal coordinate was carried out until a true local minimum was reached.

Moreover, the reliability of the present computational method was also validated by performing calculations on the first VDEs (VDE=$E_{\text{neutral at optimized anion geometry}}-E_{\text{optimized anion}}$) and the ADEs (ADE=$E_{\text{optimized neutral}}-E_{\text{optimized anion}}$). The results were compared with experimental and previous theoretical results as listed in Table 2. We can see that our calculated results agree better with the experimental results of Nakajima et al. [13] than the theoretical results calculated by Tazibt [26] using the SIESTA code based on DFT.

## Results and discussion

### Comparison of theoretical simulation and experimental photoelectron spectra

Photoelectron spectra (PES) of anion $Fe_2S_2$, $Fe_3S_4$ and $Fe_4S_4$ clusters at 266 nm (4.66 eV) photo energy were presented by Nakajima et al. [13] and are reproduced in Fig. 1a. These PES serve as definitive electronic fingerprints and allowed comparisons with theoretical simulations to locate the global minimum structures. We used three criteria in comparing the theoretical results with the experimental data to select our top-most candidate structures: (1) relative energies, (2) the first VDEs and ADEs comparing with the experimental results, (3) the relative positions of onset and (4) the first distinct peaks of simulated photoelectron spectra in the low-binding-energy range of ≤4.2 eV. The first criterion addresses the typical errors in DFT calculations, which are about a tenth of an electronvolt in the relative energies of the studied clusters.

Next, we calculated the first VDE and ADE. From Table 2, we can see that the results are in good agreement with experimental values. The VDE can reflect the ability of a molecule to lose electrons to some degree. A high vertical detachment energy implies the molecule has difficulty in losing electrons. The $Fe_3S_4$ clusters have a larger VDE (2.97 eV) and ADE (2.59 eV) than the other two clusters. Those indicate that the extra electron on $Fe_3S_4^-$ is perfect localized and hard to lose. Finally, the simulated spectra were assessed by calculating the multidimensional Franck-Condon integral. In this fashion, the Franck-Condon factors were derived for a progression of up to 20 quanta in any mode. The computed FCFs were then used to simulate the vibration structure of a neutral-to-anion state photo-detachment spectrum on the first photoelectron band of anion cluster, employing a Gaussian line-shape for each vibration component and a full-width-at-half-maximum (FWHM) of 35 meV. The simulated spectra obtained are presented in Fig. 1b. We paid particular attention to the relative position of ADE (corresponding to the slope of the first onset) and VDE (corresponding to the first peak) in the simulated spectra. The numbers of distinct peaks of simulated photoelectron spectra in the low-binding-energy range of ≤ 4.2 eV and their relative positions were also compared with the measured spectra. As seen from the Fig. 1b, the positions and the general shape of the peak are very well reproduced, but the intensity of the peak exhibits a slight difference. Nevertheless, taking into account the fact that anharmonicity effects are not included during Franck-Condon factor calculations, the overall agreement between simulated and experimental spectra is excellent.

### Geometrical structures

Since chemical reactions with clusters takes place on the cluster surface, the atomic arrangement and composition of

**Table 2** The vertical detachment energy (VDE) and adiabatic detachment energy (ADE) of the lowest energy isomer of $Fe_2S_2$, $Fe_3S_4$ and $Fe_4S_4$ clusters. For comparison, we also list available experimental and other theoretical data

| Cluster | VDE (eV) | | ADE (eV) | |
|---|---|---|---|---|
| | Theory | Experimental [13] | Theory | Experimental [13] |
| $Fe_2S_2$ | 2.07 | 2.39±0.13 | 2.02 | 2.15±0.83 |
| | 0.81 [26] | | 0.80 [26] | |
| | 1.37 [24] | | 1.20 [24] | |
| $Fe_3S_4$ | 2.97 | 3.47±0.14 | 2.59 | 3.22±0.33 |
| | 1.21 [26] | | 1.06 [26] | |
| $Fe_4S_4$ | 2.24 | 2.27±0.06 | 2.08 | 2.04±0.04 |
| | 1.34 [26] | | 1.15 [26] | |

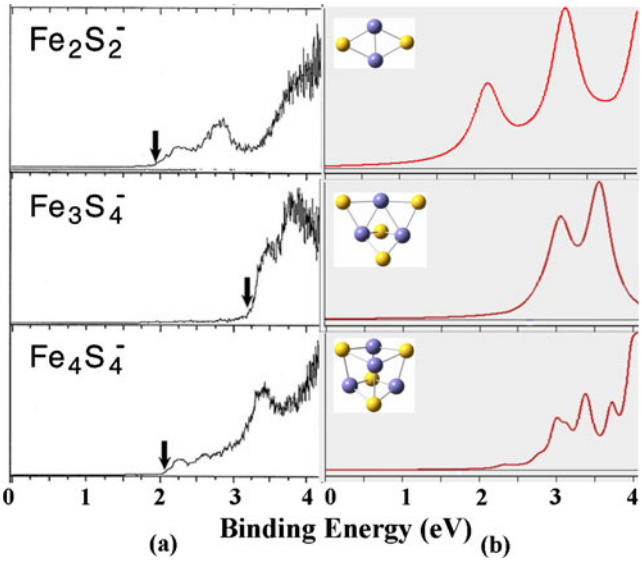


**Fig. 1** **a** Photoelectron spectra of $Fe_2S_2^-$, $Fe_3S_4^-$ and $Fe_4S_4^-$ clusters measured at 266 nm (4.66 eV). The spectra are taken from [13]. **b** Simulated photoelectron spectra on the first photoelectron band of the lowest energy structures for the anion at the B3PW91/6-311+G* level

the surface play an important role. The starting point in any description of cluster properties is their geometrical structure. To our knowledge, there are only a few preliminary studies on neutral and charged $Fe_2S_2$, $Fe_3S_4$ and $Fe_4S_4$ isolated clusters [24–26]. The details of the electronic structures and their geometric structures are still unclear. Thus, we were interested in further investigating the geometrical structure of freestanding $Fe_2S_2$, $Fe_3S_4$, and $Fe_4S_4$ clusters. Among other properties, we also examined detailed point symmetry, electronic state, spin multiplicity. Compared with most experimental suggestions concerning possible geometric structures, we found that the ground state geometries of the freestanding $Fe_2S_2$, $Fe_3S_4$, and $Fe_4S_4$ clusters are similar to that when they are present in proteins, which was again confirmed in our subsequently obtained geometries. Using the computation scheme described in the section on Computational methods, we obtained a large number of low-lying isomers and determined the ground state structures for $Fe_2S_2^{0/-}$, $Fe_3S_4^{0/-}$ and $Fe_4S_4^{0/-}$ clusters. They were optimized at B3PW91/6-311+G* level and are presented in Fig. 2. According to the total energies from low to high, these isomers are designated *n*a/*n*a*, *n*b/*n*b*, *n*c/*n*c*, *n*d/*n*d*, and *n*e/*n*e* for the neutral and anion clusters, respectively. ("*n*" is the number of Fe atoms in the studied clusters). Their corresponding symmetry, electronic state, relative energy and the vibration frequencies with the greatest IR intensities are summarized in Table 3. We believe that we have identified the geometrical structures of freestanding $Fe_2S_2^{0/-}$, $Fe_3S_4^{0/-}$ and $Fe_4S_4^{0/-}$ clusters correctly. This belief is based on our ability to explain the (both vertical and adiabatic) detachment energies and electronic properties consistently and quantitatively.

### $Fe_2S_2^{0/-}$

The optimized structures show that the geometrical structures of the neutral and anionic $Fe_2S_2$ clusters are similar, but with small distortions. This may be due to the fact that gaining an electron has little influence on their structure. The ground state of $Fe_2S_2$ and $Fe_2S_2^-$ clusters, in which the two iron atoms locate in the short diagonal (see Fig. 2), favors higher spin states. This differs from Hübner's results [24, 25], which show that the ground state of neutral $Fe_2S_2$ is $^1A_1$. The second low-lying isomer has a $^9A'$ electronic state and is only 0.37 eV lower in total energy. However, in our optimized calculations, we found that the nonet state is the ground state. The choice of functional has a sensitive influence on the physical parameters that are computed. Such small relative energy differences make it difficult to distinguish the ground state accurately. Our calculated VDE and ADE of the ground state isomer are in better agreement with the experimental value, so we believe that our result is reliable. The closed rhombic structure is more stable than the open/linear chain structure, and each sulfur atom has two bonds in this ground state geometry, which is similar to that forming in some protein cores [49–52]. Thus, we think that this is actually the building block for large Fe-S cores in proteins. For the $Fe_2S_2^-$ cluster, the ground state is $^8B_{1g}$, which has a Fe–Fe distance of 2.11 Å. The spin state is consistent with the result of Hübner [25]. Additionally, it worth pointing out that the binding energy per atom $E_b\left(Fe_xS_y^{\mu}\right) = [xE(Fe) + (y-1)E(S) + E(S^{\mu}) - E\left(Fe_xS_y{}^{\mu}\right)]/(x+y)$ is 2.67 eV, which is smaller than that of neutral cluster (2.69 eV). This indicates that attachment of an extra electron to the ground state of $Fe_2S_2$ results in an anion $Fe_2S_2^-$ cluster, which is less stable than the neutral cluster.

### $Fe_3S_4^{0/-}$

In our calculations, the $Fe_3S_4$ cluster can be obtained by removing one Fe atom from the cubane $Fe_4S_4$ geometry. Here, we also confirm that the ground state geometry of $Fe_3S_4$ is similar to their structure in proteins [49–52]. From Fig. 2, one can see that all of the structures can be classified into two types based on their shapes: (1) an interior Fe trimer cluster surrounded by S atoms, and (2) a structure consisting of two $Fe_2S_2$ entities of rhombic structure with one common

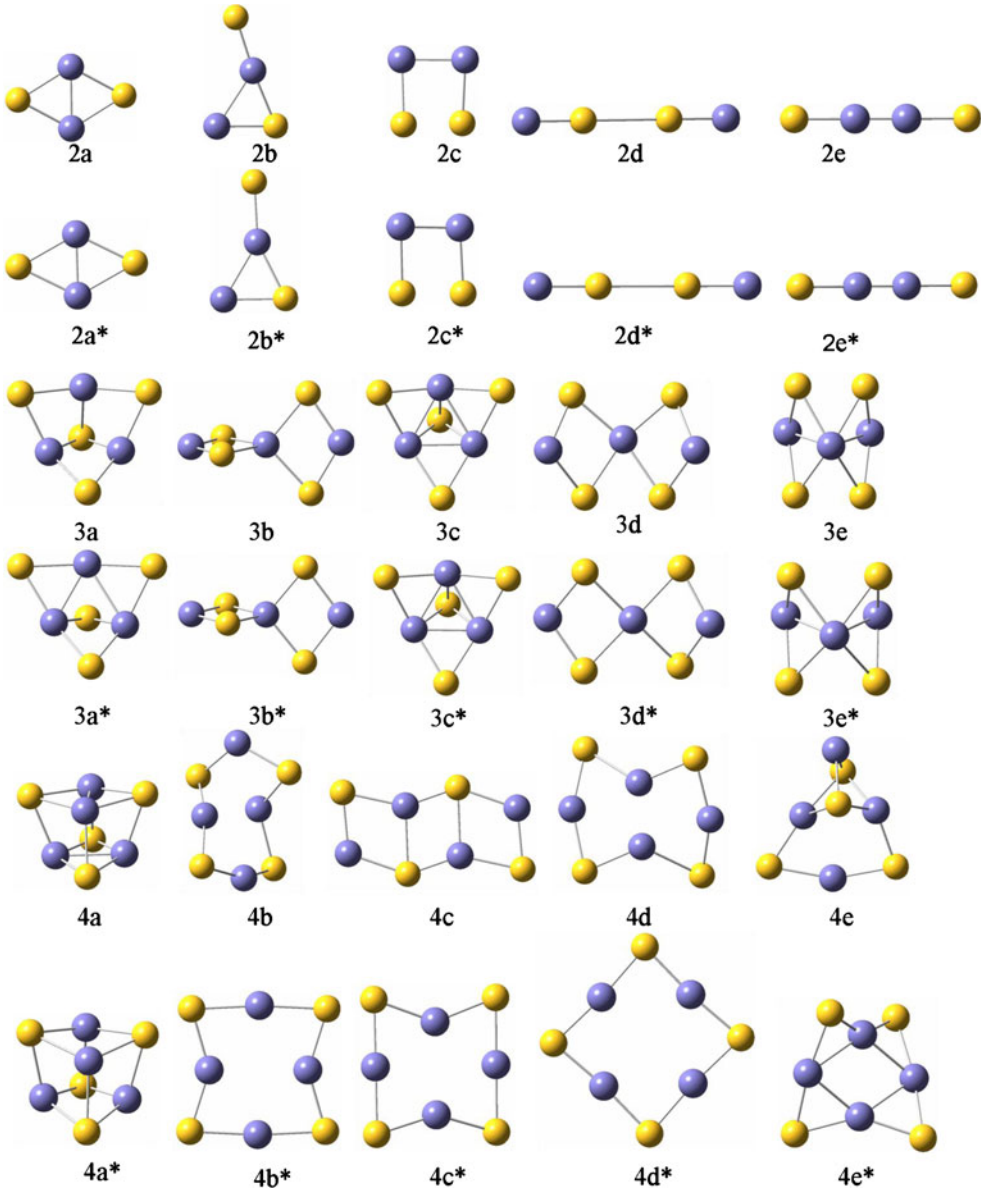


**Fig. 2** Lowest energy and low-lying structures of $Fe_2S_2^{0/-}$, $Fe_3S_4^{0/-}$ and $Fe_4S_4^{0/-}$ clusters as presented by the B3PW91 functional. Isomers are designated *n*a/*n*a*, *n*b/*n*b*, *n*c/*n*c*, *n*d/*n*d*, and *n*e/*n*e* for the neutral and anion clusters, respectively. *Yellow* and *blue balls* represent sulfur and iron atoms, respectively

Fe atom (perpendicular and parallel). In addition, we found that the sulfur atoms tend to form the maximum number of bonds with Fe, and the point symmetry for the neutral isomers is the same as that of the corresponding anions (3a→3a*, 3b→3b*, 3c→3c* and 3e→3e*) except for 3d→3d*. Just like $Fe_2S_2^{0/-}$ clusters, the ground state $Fe_3S_4^{0/-}$ also favors high spin state ($^{11}$A and $^{10}$A, respectively). The calculated $E_b$ values are 3.03 and 3.13 eV for $Fe_3S_4^{0/-}$, respectively, indicating that they are more stable than $Fe_2S_2^{0/-}$ clusters.

### *$Fe_4S_4^{0/-}$*

The ground state structure (4a with $D_{2d}$ point symmetry) of the $Fe_4S_4$ cluster is a distorted cube structure in which Fe and S atoms are at alternate vertices, and each face is a stable planar rhombus. Similarly, the geometry structure of ground state anionic $Fe_4S_4^-$ cluster is similar to that of the neutral cluster. This means that the gas phase $Fe_xS_y^-$ ion structures ($y=x$ or $y=x\pm1$) built from FeS pairs or $Fe_2S_2$ rhombs are logical, and it also means that Fe and S atoms have the same average coordinate numbers. In addition, we found that the structures for the larger Fe-S clusters ($Fe_3S_4^{0/-}$ and $Fe_4S_4^{0/-}$) prefer a closed geometry. This may be explained by the fact that in pure $Fe_n$ clusters [53] p–d bonding is not directional and more closed geometries are obtained for $n\geq4$. Whereas the pure sulfur clusters favor open or ring-like geometries due to directional p–p bonding [45, 54]. Furthermore, according to some previous publications [49–52], the $Fe_4S_4$ cluster in neutral and anionic state retains this cubane-like geometry when present in proteins. The calculated $E_b$ shows that the neutral $Fe_4S_4$ cluster is more stable than its anionic state.

**Table 3** Geometries, symmetries (Sym), electron state (State), relative energies ($\Delta E$) and the vibration frequencies (Freq) with greatest IR intensities of the $Fe_2S_2^{0/-}$, $Fe_3S_4^{0/-}$ and $Fe_4S_4^{0/-}$ clusters

| Isomer | Sym | State | $\Delta E$ (eV) | Freq ($cm^{-1}$) | Isomer | Sym | State | $\Delta E$(eV) | Freq ($cm^{-1}$) |
|---|---|---|---|---|---|---|---|---|---|
| 2a | $D_{2h}$ | $^9B_{1g}$ | 0.00 | 227, 447, 446 | 2a* | $D_{2h}$ | $^8B_{1g}$ | 0.00 | 116, 216, 433 |
| 2b | $C_s$ | $^7A''$ | 1.23 | 54, 259, 411, 495 | 2b* | $C_s$ | $^6A''$ | 1.37 | 166, 235, 448 |
| 2c | $C_2$ | $^9A$ | 2.34 | 59, 330, 367, 458 | 2c* | $C_s$ | $^8A''$ | 2.67 | 236, 315, 432 |
| 2d | $D_{\infty h}$ | $^{11}A$ | 5.09 | 19, 19, 491 | 2d* | $D_{\infty h}$ | $^{10}A$ | 3.47 | 16, 16, 449 |
| 2e | $D_{\infty h}$ | $^3\sum_g$ | 6.61 | 51, 51, 592 | 2e* | $C_{\infty h}$ | $^4\sum$ | 4.98 | 57, 162, 402 |
| 3a | $C_s$ | $^{11}A$ | 0.00 | 164, 194, 338, 410, 462 | 3a* | $C_s$ | $^{10}A$ | 0.00 | 153, 221, 392, 425, 445 |
| 3b | $D_{2d}$ | $^7B_1$ | 0.51 | 215, 287, 452, 500, 500 | 3b* | $D_{2d}$ | $^8B_2$ | 1.51 | 32, 202, 274, 274, 371 |
| 3c | $C_{3v}$ | $^9A$ | 1.07 | 399, 419, 421, 498, 573 | 3c* | $C_{3v}$ | $^6A_2$ | 1.82 | 172, 172, 403, 452, 452 |
| 3d | $C_1$ | $^{11}A$ | 1.60 | 125, 157, 308, 318, 451 | 3d* | $C_s$ | $^8A'$ | 2.50 | 181, 274, 299, 434, 463 |
| 3e | $C_{2v}$ | $^9B_1$ | 2.20 | 113, 131, 175, 199, 433 | 3e* | $C_{2v}$ | $^8A$ | 2.66 | 150, 233, 253, 356, 399 |
| 4a | $D_{2d}$ | $^{11}A$ | 0.00 | 191, 204, 249, 378, 396, 404 | 4a* | $D_{2d}$ | $^{10}B_g$ | 0.00 | 210, 222, 252, 368, 380, 382 |
| 4b | $C_1$ | $^9A$ | 1.10 | 196, 316, 382, 426, 448, 475 | 4b* | $D_{2h}$ | $^6A''$ | 1.02 | 95, 115, 174, 301, 433, 458 |
| 4c | $C_{2h}$ | $^9A$ | 1.30 | 195, 278, 290, 380, 447, 448 | 4c* | $C_2$ | $^{10}B_{2g}$ | 2.28 | 96, 162, 293, 439, 462, 480 |
| 4d | $C_2$ | $^7A$ | 1.66 | 133, 202, 325, 436, 449, 470 | 4d* | $D_{4h}$ | $^8A$ | 2.83 | 93, 154, 296, 444, 460 |
| 4e | $C_s$ | $^{11}A$ | 4.54 | 173, 225, 271, 418, 425, 431 | 4e* | $D_2$ | $^{10}A$ | 2.89 | 86, 104, 158, 437, 463, 479 |

## Electronic properties

### *HOMO-LUMO gaps*

The electronic properties of the $Fe_2S_2^{0/-}$, $Fe_3S_4^{0/-}$ and $Fe_4S_4^{0/-}$ clusters can be discussed by examining the highest occupied–lowest unoccupied molecular orbital (HOMO–LUMO) energy gap (HLG). The HLG is a useful quantity for examining cluster stability. It reflects the ability of electrons to jump from occupied orbital to unoccupied orbitals and represents the ability of the molecule to participate in chemical reactions to some degree. In other words, a large value of the HLG is related to an enhanced chemical stability. For the most stable $Fe_2S_2^{0/-}$, $Fe_3S_4^{0/-}$ and $Fe_4S_4^{0/-}$ clusters, the frontier molecular orbital (FMO) energies and HOMO–LUMO gaps are listed in Table 4. The FMO contour maps are plotted in Fig. 3. These MOs provide insight into the observed the electron delocalization pattern for all the clusters and the nature of bonding between Fe-S clusters.

**Table 4** Binding energies ($E_b$) per atom, highest occupied molecular orbital (HOMO), lowest unoccupied molecular orbital (LUMO) and HOMO–LUMO energy gaps (HLG) for the ground state of the $Fe_2S_2^{0/-}$, $Fe_3S_4^{0/-}$ and $Fe_4S_4^{0/-}$ clusters

| Cluster | $E_b$(eV) | HOMO (eV) | LUMO (eV) | HLG (eV) |
|---|---|---|---|---|
| 2a | 2.69 | −5.86 | −3.99 | 1.86 |
| 2a* | 2.67 | −3.13 | 1.60 | 1.92 |
| 3a | 3.03 | −6.76 | −5.33 | 1.42 |
| 3a* | 3.13 | −2.02 | −0.18 | 1.34 |
| 4a | 3.35 | −4.78 | −4.24 | 0.54 |
| 4a* | 3.06 | −0.81 | 0.07 | 0.88 |

As can be seen from Fig. 3 and Table 4: (1) in the $Fe_2S_2$ (2a) cluster, the spin-down HOMO (β) has higher energy than the spin-up HOMO (α). The HOMO (β) has significant p character on all S atoms, and large d and considerable p character on Fe atoms, leading to a bonding interaction between the atoms of the long diagonal S and short diagonal Fe atoms; the LUMO (β) involves mainly the large d and considerable p orbital of the Fe atoms. While for the anionic $Fe_2S_2$ (2a*) cluster, the only difference is that the HOMO are composed of minor s and significant p orbital from sulfur atoms. Additionally, we found that the HLG of anionic $Fe_2S_2$ is larger than that of neutral $Fe_2S_2$. This may be related to the π-bonding interaction between iron-d and sulfur-s orbitals maximizing the chemical stability. (2) To probe further into the bonding properties, we examined the composition of the HOMO and some LUMOs. For the ground state $Fe_3S_4$, the HOMO involves mostly s (3.80%), p (3.70%), d (92.50%) from the three Fe atoms, and large p and considerable s orbitals from the four S atoms. The α77-LUMO consists of Fe-p (4.16%), Fe-d (92.01%), Fe-s (3.83%) and S-p (99.89%) orbitals. For $Fe_3S_4^-$, the β67-HOMO is composed of Fe-s (3.02%), Fe-p (6.93%), Fe-d (91.05%) and significant S-p. The LUMO is an α type molecular orbital, whose irreducible representation is $a_u$. (3) In the case of $Fe_4S_4$ and $Fe_4S_4^-$ clusters, we also investigated the electronic structure and distribution of their HOMOs. $Fe_4S_4$: the d content (91.66 %) always tends to be the major component of the HOMOs for Fe atoms, and the sulfur atoms are always *p*-like (94.04 %). $Fe_4S_4^-$: the HOMO involves mainly iron s (3.49 %), p (3.39 %), d (93.12 %); sulfur s (0.91 %), d (0.29 %) and p (98.80 %). All in all, we found both the HOMO and LUMO of neutral

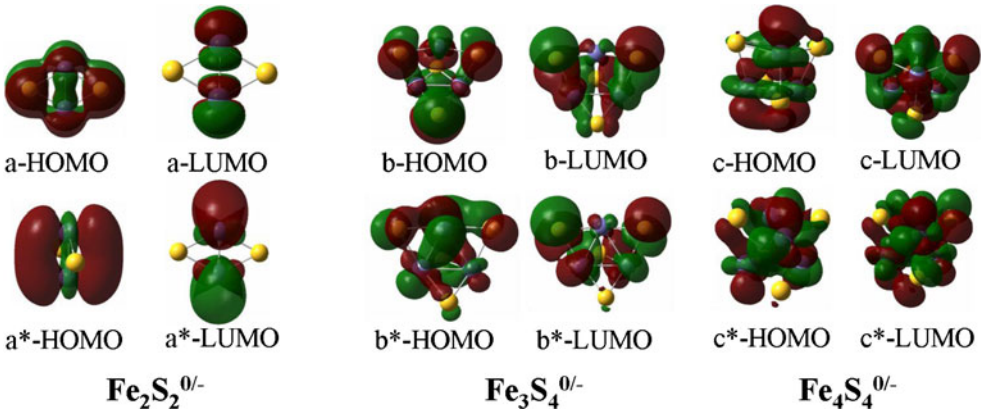


**Fig. 3** Highest occupied (HOMO) and lowest unoccupied molecular orbital (LUMO) contour structures of neutral and anionic $Fe_2S_2$, $Fe_3S_4$ and $Fe_4S_4$ clusters (isovalue=0.02au). *Top line* Neutral isomer, *bottom line* anions

and anionic clusters to involve mainly the d orbital from the iron atoms and the p orbital from sulfur atoms. These molecular orbitals indicate that p–d hybridization occurs between the Fe and S atoms, which would impact the geometrical structures and the stability of the clusters.

*Natural population analysis and electronic density difference*

In order to more fully understand the electronic properties of the neutral and anionic $Fe_2S_2$, $Fe_3S_4$, and $Fe_4S_4$ clusters, natural population analysis (NPA) was performed. NPA can provide a reasonable explanation of the charge transfer within the cluster. The calculated results for the ground state are summarized in Table 5; we can clearly see that all of the sulfur atoms in $Fe_2S_2^{0/-}$, $Fe_3S_4^{0/-}$ and $Fe_4S_4^{0/-}$ clusters possess negative charges, while the iron atoms have positive charges. This indicates that electrons transfer from Fe atoms to S atoms, namely, iron atoms act as electron donors in all clusters. This may be due to the electronegativity of S (2.58) is much larger than that of Fe (1.83), and the sulfur atom has a stronger ability to attract electrons. In addition, it is interesting to find that two sulfur atoms located at the same site on the identical cluster have equal charges, i.e., the charge distribution is dependent on the symmetry of cluster.

Meanwhile, aiming at probing into the redistribution of electron density induced by bonding and charge transfer nature in detail, the electron density differences were taken into account and calculated by the program Multiwfn [55]. The maps for investigated $Fe_2S_2^{0/-}$, $Fe_3S_4^{0/-}$ and $Fe_4S_4^{0/-}$ clusters are sketched in Fig. 4. The electron density difference can provide qualitative information on the electron flow over the whole complex. As observed in the contour line diagrams of Fig. 4, the solid lines indicate areas of excess electron concentration in which the electron density difference has a positive value ($\Delta\rho>0$), while the dashed lines show that the electron density difference of the regions is negative ($\Delta\rho<0$) where electrons decrease. Because most of the ground states for selected clusters are three-dimensional (3D) structures, we generated contour line diagrams in two dimensions (2D) using 200, 200 grids in two ways to clearly reflect electron flow: (1) plotting maps in the YZ plane; and (2) defining a plane by three atoms, e.g. 1Fe, 2Fe, 3Fe atoms and so on. Additionally, the geometrical structures in Cartesian coordinates and the labels of atoms were also calculated to gain a better view.

It can be seen clearly from the maps in Fig. 4 that the electron density difference increased significantly in the bonding region between Fe and S atoms called the shift-centered electron. This may be due to the covalent component in the bonding. For the neutral and anionic $Fe_2S_2$ clusters, we found that most electrons spread out from the side of the sulfur atom, indicating that the lone pair density in the sulfur atom is more diffuse. This is more apparent for the $Fe_2S_2^-$ cluster and is in good agreement with natural population analysis (S atoms possess −0.8882 electron charges in $Fe_2S_2^-$, while they have − 0.6934 electron in $Fe_2S_2$). As with $Fe_3S_4$ and $Fe_3S_4^-$ clusters, they have a Fe

**Table 5** Natural charge populations of the lowest energy $Fe_2S_2^{0/-}$, $Fe_3S_4^{0/-}$ and $Fe_4S_4^{0/-}$ clusters

| Cluster | Fe-1 | Fe-2 | Fe-3 | Fe-4 | S-5 | S-6 | S-7 | S-8 |
|---|---|---|---|---|---|---|---|---|
| $Fe_2S_2$ | 0.6934 | 0.6934 | | | −0.6934 | −0.6934 | | |
| $Fe_3S_4$ | 0.3741 | 0.2064 | 0.2064 | | −0.2245 | −0.2216 | −0.2730 | −0.0681 |
| $Fe_4S_4$ | 0.2099 | 0.1624 | 0.2013 | 0.1765 | −0.1955 | −0.1762 | −0.1946 | −0.1840 |
| $Fe_2S_2^-$ | 0.3882 | 0.3882 | | | −0.8882 | −0.8882 | | |
| $Fe_3S_4^-$ | 0.3195 | 0.1168 | 0.1304 | | −0.4499 | −0.4726 | −0.4653 | −0.1790 |
| $Fe_4S_4^-$ | 0.3654 | 0.1872 | 0.3125 | 0.2912 | −0.4760 | −0.5040 | −0.5897 | −0.5866 |

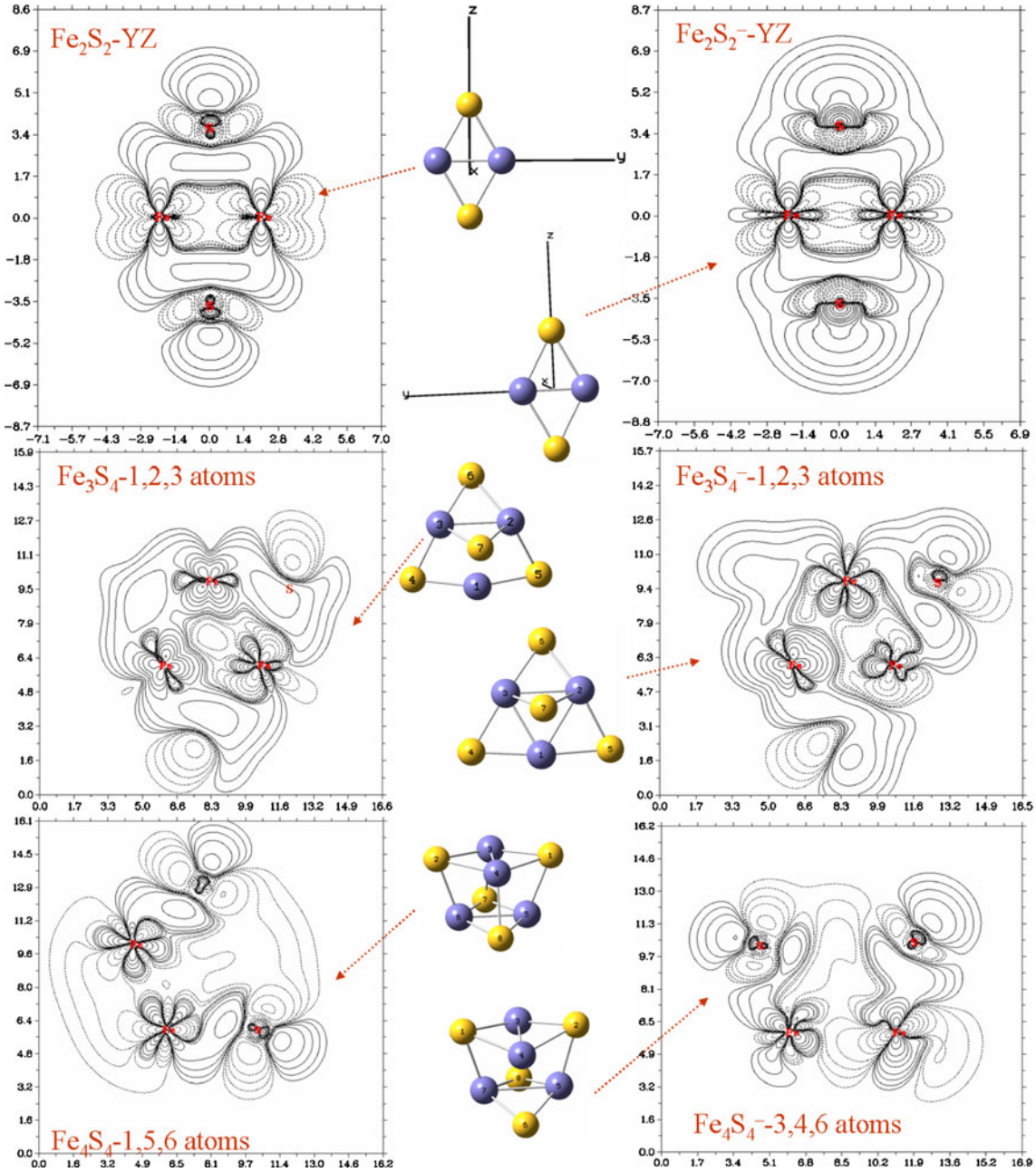


**Fig. 4** Electron density difference contour line maps of ground state $Fe_2S_2^{0/-}$, $Fe_3S_4^{0/-}$ and $Fe_4S_4^{0/-}$ clusters in a two-dimensional (2D) YZ and three atoms plane. All maps are drawn in the same scale of length Bohr unit (1 Bohr=0.529172 Å)

trimer cluster surrounded by S atoms. The geometrical structures allow many electrons to be attracted easily by the surrounding sulfur atoms. Thus, it is not surprising to find that the electrons around iron atoms decrease, especially in the first Fe atom, as also confirmed by NPA. In the case of $Fe_4S_4$ and $Fe_4S_4^-$ clusters, the phenomenon of electron flow is similar to that of $Fe_2S_2^{0/-}$ and $Fe_3S_4^{0/-}$ clusters. Most electrons also transfer from the Fe atoms to S atoms and the electron density difference increases significantly in the bonding region between Fe and S atoms.

## Magnetic properties

Magnetism is one of the most prominent properties of transition metals. Among the 3d transition metal elements, it is well known the Fe, Co and Ni are ferromagnetic in the standard bulk phases. It is an interesting problems to elucidate how magnetic moments can be affected further if transition metal atoms bond with other elements. Thus, based on the optimized geometries, the magnetic properties of the lowest energy

structures for neutral and anionic $Fe_2S_2$, $Fe_3S_4$, and $Fe_4S_4$ clusters were studied. The results (Table 6) clearly show that the total magnetic moments of neutral and anionic clusters are in the range of 7.98 to 10.27 $\mu_B$ and 7.02 to 9.61 $\mu_B$, respectively, and locate mainly on Fe (7.26−10.02 $\mu_B$ and 6.52−9.28 $\mu_B$, respectively) atoms. Only very small amounts of spin (about 0.25−0.72 $\mu_B$ and 0.33−0.64 $\mu_B$) are found on the S sites. To investigate further the contributions of iron and sulfur atoms to the total magnetic moments, the local magnetic moments of 3d, 4s, 4p states for Fe and 3s, 3p, 3d states for S atoms were analyzed. We found that the local magnetic moment of iron atoms is due mainly to the 3d state, whereas the 3p orbital contributes the biggest effect for sulfur atoms. We guess that the magnetic properties of clusters are also related to a strong p–d orbital interaction.

In addition, electron density from spin self consistent field (SCF) density (isovalue=0.004au) maps are also performed and plotted in Fig. 5. The spin density maps directly predict the spin densities for all complexes included in this study. As can be seen clearly from Fig. 5, the color of the transparent envelopes change gradually from blue to green. Blue transparent envelope represents positive spin density, while green envelope corresponds to negative spin density. Thus, in the clusters considered here, the spin densities reside mainly on the iron atoms. This is also confirmed by the results of the calculated magnetic moment on donor Fe atoms, which is listed in Table 6. Again, we can detect the existence of small green regions of negative spin density at the midpoint of iron–iron bonds and the iron trimer. Furthermore, Fig. 5 shows that the blue region is more obvious than the green region, indicating that the spin quantum number J≠0 and that these systems are ferromagnetic. Unfortunately, there are no available experimental values to date for comparison for $Fe_2S_2^{0/-}$, $Fe_3S_4^{0/-}$ and $Fe_4S_4^{0/-}$, thus our theoretical results need to be verified further by experiments.

**Table 6** Magnetic moment of Fe and S atoms [Fe ($\mu_B$) and S ($\mu_B$)], and the total magnetic moment ($\mu_B$) for the lowest energy structures of $Fe_2S_2^{0/-}$, $Fe_3S_4^{0/-}$ and $Fe_4S_4^{0/-}$ clusters

| Cluster | Magnetic moment on Fe ($\mu_B$) | Magnetic moment on S ($\mu_B$) | Total magnetic moment ($\mu_B$) |
|---|---|---|---|
| $Fe_2S_2$ | 7.26 | 0.72 | 7.98 |
| $Fe_3S_4$ | 9.34 | 0.61 | 9.95 |
| $Fe_4S_4$ | 10.02 | 0.25 | 10.27 |
| $Fe_2S_2^-$ | 6.52 | 0.50 | 7.02 |
| $Fe_3S_4^-$ | 8.94 | 0.64 | 9.58 |
| $Fe_4S_4^-$ | 9.28 | 0.33 | 9.61 |

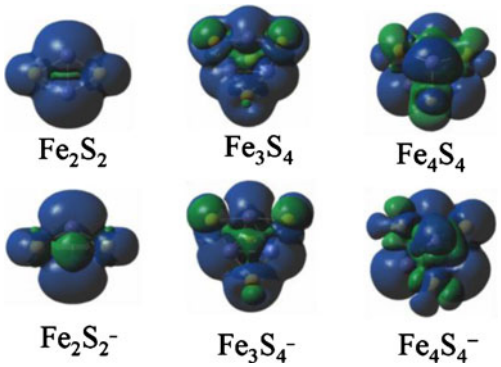


**Fig. 5** Electron density from spin self consistent field (SCF) density (isovalue=0.004au) maps for the lowest energy structures of $Fe_2S_2^{0/-}$, $Fe_3S_4^{0/-}$ and $Fe_4S_4^{0/-}$ clusters. *Blue* Positive spin density, *green* negative spin density

## Conclusions

Summarizing, we have identified the ground state geometries and studied the electronic and magnetic properties of neutral and anionic $Fe_2S_2$, $Fe_3S_4$, and $Fe_4S_4$ clusters by means of all electron calculations realized with B3PW91/6-311+G* method. From the above studies, we draw the following conclusions:

(1) The ground state structures and low-lying isomers of neutral and anion species were obtained using both the relative energies and comparisons between the simulated spectra and experimental PES data. Furthermore, the VDE and ADE were calculated and compared with experimental results to verify the ground state, and good agreement was achieved. The ground state structures for neutral and anionic $Fe_2S_2$, $Fe_3S_4$ and $Fe_4S_4$ clusters are very similar, but with small distortions. All favor a high spin state and are similar to their structure in proteins.

(2) FMOs were studied to explain the electron delocalization pattern for all the clusters and the nature of bonding between Fe and S atoms. The d content of Fe atoms always tends to be the major component of HOMOs and the sulfur atoms in the investigated clusters were always p-like. This was also confirmed by HOMO and LUMO contour map analysis.

(3) According to NPA, it was noted that Fe atoms act as electron donors in the corresponding $Fe_2S_2^{0/-}$, $Fe_3S_4^{0/-}$ and $Fe_4S_4^{0/-}$ configurations, and the charge distribution is dependent on the symmetry of cluster. In addition, electron density difference maps show the direction of electron flow over the whole complex. Many electrons are attracted by sulfur atoms, which is consistent with NPA. We also found that the electron density difference increased significantly in the bonding region between Fe and S atoms.

(4) The magnetism of $Fe_2S_2^{0/-}$, $Fe_3S_4^{0/-}$ and $Fe_4S_4^{0/-}$ clusters was studied by calculating the total magnetic moment and the magnetic moment on each type of atom. Iron atoms carried most of the magnetic moments and only very small magnetic moments were found on sulfur atoms. The local magnetic moment of iron atoms is due mainly to the 3d state, whereas that of S atoms is due to the 3p state. Spin densities for all complexes included in this study were also mainly located on transition metal Fe atoms.

**Acknowledgments** This work was supported by the National Natural Science Foundation of China (No. 10974138 and No. 11104190) and the Doctoral Education Fund of Education Ministry of China (No. 20100181110086 and No. 20111223070653).

## References

1. Rees DC, Howard JB (2003) Science 300:929–931
2. Johnson MK (1994) In: King RB (ed) Encyclopedia of inorganic chemistry. Wiley, Chichester, 1896–1915
3. Beinert H, Holm RH, Münck E (1997) Science 277:653–659
4. Johnson MK (1998) Curr Opin Chem Biol 2:173–181
5. Beinert H, Kiley PJ (1999) Curr Opin Chem Biol 3:152–157
6. Beinert H (2000) J Biol Inorg Chem 5:2–15
7. Matsubara H, Hase T, Wakabayashi S, Wada K (1980) In: Sigman DS, Brazier MA (eds) The evolution of protein structure and function. Academic, New York
8. Lovenberg W (1973–1977) Iron-sulfur proteins. Academic, New York
9. Spiro TG (1982) Iron-sulfur protein. Wiley, New York
10. Beinert H (1990) FASEB J 4:2483–2491
11. Cammack R (1992) Advances in inorganic chemistry. Academic, New York
12. Mulder DW, Boyd ES, Sarma R, Lange RK, Endrizzi JA, Broderick JB, Peters JW (2010) Astrobiology Science Conference. League City, TX
13. Nakajima A, Hayase T, Hayakawa F, Kaya K (1997) Chem Phys Lett 280:381–389
14. Zhang N, Hayase T, Kawamata H, Nakao K, Nakajima A, K K (1996) J Chem Phys 104:3413–3419
15. Bililign S, Feigerle CS, Miller JC (1998) Appl Surf Sci 344:127–129
16. Whetten RL, Cox DM, Trevor DJ, Kaldor A (1985) J Phys Chem 89:566–569
17. Torres RA, Lovell T, Noodleman L, Case DA (2003) J Am Chem Soc 125:1923–1936
18. Bhave DP, Han WG, Pazicni S, Penner-Hahn JE, Carroll KS, Noodleman L (2011) Inorg Chem 50:6610–6625
19. Dey A, Glaser T, Moura JJG, Holm RH, Hedman B, Hodgson KO, Solomon EI (2004) J Am Chem Soc 126:16868–16878
20. Jensen KP (2008) J Inorg Biochem 102:87–100
21. Sigfridsson E, Olsson MHM, Ryde U (2001) Inorg Chem 40:2509–2519
22. Li (2000) J Acta Chem Sinica 58:1529–1533
23. Knottenbelt SZ, McGrady JE (2003) J Am Chem Soc 125:9846–9852
24. Hübner O, Sauer J (2002) J Chem Phys 116:617–628
25. Hübner O, Sauer J (2002) Phys Chem Chem Phys 4:5234–5243
26. Tazibt S, Bouarab S, Ziane A, Parlebas JC, Demangeat C (2010) J Phys B: At Mol Opt Phys 43:165101–165109
27. Frisch MJ, Trucks GW, Schlegel HB, Scuseria GE, Robb MA, Cheeseman JR, Montgomery JA, Jr, Vreven T, Kudin KN, Burant JC, Millam JM, Iyengar SS, Tomasi J, Barone V, Mennucci B, Cossi M, Scalmani G, Rega N, Petersson GA, Nakatsuji H, Hada M, Ehara M, Toyota K, Fukuda R, Hasegawa J, Ishida M, Nakajima T, Honda Y, Kitao O, Nakai H, Klene M, Li X, Knox JE, Hratchian HP, Cross JB, Bakken V, Adamo C, Jaramillo J, Gomperts R, Stratmann RE, Yazyev O, Austin AJ, Cammi R, Pomelli C, Ochterski JW, Ayala PY, Morokuma K, Voth GA, Salvador P, Dannenberg JJ, Zakrzewski VG, Dapprich S, Daniels AD, Strain MC, Farkas O, Malick DK,Rabuck AD, Raghavachari K, Foresman JB, Ortiz JV, Cui Q, Baboul AG, Clifford S, Cioslowski J, Stefanov BB, Liu G, Liashenko A, Piskorz P, Komaromi I, Martin RL, Fox DJ, Keith T, Al-Laham MA, Peng CY, Nanayakkara A, Challacombe M, Gill PMW, Johnson B, Chen W, Wong MW, Gonzalez C (2004) J A Pople, Gaussian 03, Revision E.01. Gaussian Inc, Wallingford, CT
28. Wilson S (1987) Adv Chem Phys 167:474–483
29. Schröder D, Kretzschmar N, Schwaz H, Rue C, Armentrout PB (1999) Inorg Chem 38:3474–3480
30. Becke AD (1993) J Chem Phys 98:5648–5652
31. Perdew JP, Ziesche P, Eschrig H (eds) (1991) Electronic structure of solids. Akademie, Berlin
32. Lee CT, Yang WT, Parr RG (1988) Phys Rev B 37:785–789
33. Perdew JP, Burke K, Ernzerhof M (1996) Phys Rev Lett 77:3865–3868
34. Perdew JP (1986) Phys Rev B 33:8822–8824
35. Zhai HJ, Kiran B, Wang LS (2003) J Phys Chem A 107:2821–2828
36. Huber KP, Herzberg G (1979) Molecular spectra and molecular structure IV; Constants of diatomic molecules. Van Nostrand Reinhold, New York
37. Hüber KP, Herzberg G (1974) Molecular spectra and molecular structure IV; Constants of diatomic molecules. Van Nostrand Reinhold, New York
38. Hunsicker S, Jones RO, Gantefor G (1995) J Chem Phys 102:5917–5936
39. Hohl D, Jones RO, Car R, Parrinello M (1988) J Chem Phys 89:6823–6835
40. Lian CX, Su, Armentrout PB (1992) J Chem Phys 97:4072–4083
41. Purdum H (1982) Phys Rev B 25:4412–4417
42. Moskovits M, DiLella DP (1980) J Chem Phys 73:4917–4924
43. Barrow RF, Cousins C (1971) Adv High Temp Chem 4:161–170
44. Devore TC, Franzen HF (1975) High Temp Sci 7:220–235
45. Jones RO, Ballone P (2003) J Chem Phys 118:9257–9265
46. Raghavachari K, Rohlfing CM, Stephen J (1990) J Chem Phys 93:5862–5874
47. Chen MD, Liu ML, Zheng LS, Zhang QE, Au CT (2001) Chem Phys Lett 350:119–127
48. Hunsicker S, Jones RO, Ganteför G (1995) J Chem Phys 102:5917–5936
49. Mayerle JJ, Denmark SE, DePamphilis BV, Ibers JA, Holm RH (1975) J Am Chem Soc 97:1032–1045
50. Krebs C, Agar JN, Smith AD, Frazzon J, Dean DR, Huynh BH, Johnson MK (2001) Biochemistry 40:14069–14080
51. Johnson MK, Staples CR, Duin EC, Lafferty ME, Duderstadt RE (1988) Appl Chem 70:939–946
52. Rotsaer FAJ, Pikus JD, Fox BG, Markley JL, Sanders-Loehr J (2003) J Biol Inorg Chem 8:318–326
53. Diéguez O, Alemany MMG, Rey C, Ordejón P, Gallego LJ (2001) Phys Rev B 63:205407
54. Millefiori S, Alparone A (2001) J Phys Chem A 105:9489–9497
55. Lu, T. Multiwfn, version 2.1.2. http://multiwfn.codeplex.com/